A metamaterial-inspired, electrically small rectenna for high-efficiency, low power harvesting and scavenging at the global positioning system L1 frequency

Ning Zhu, Richard W. Ziolkowski,[a)] and Hao Xin
Department of Electrical and Computer Engineering, University of Arizona, 1230 E. Speedway Blvd., Tucson, Arizona 85721-0104, USA

An electrically small rectenna was designed and tested at the global positioning system (GPS) L1 frequency (1.5754 GHz). The metamaterial-inspired near-field resonant parasitic antenna size (ka $\sim$ 0.467) and its direct match to the input impedance of the rectifying circuit decreased the whole size of the rectenna (ka $\sim$ 0.611). The simulated and measured rectifying efficiencies were, respectively, 75.7% and 79.6% when the input power to the rectifying circuit was 0.0 dBm (1 mW). The highest rectifying efficiency, 84.7%, was achieved at the GPS L1 frequency for a 3.0 dBm input power. The simulated and measured results are in good agreement. © *2011 American Institute of Physics*. [doi:10.1063/1.3637045]

Rectennas, which is short for rectifying antennas, have received much attention for their use in wireless power transmission (WPT) systems.[1,2] They are promising elements for power harvesting and scavenging, especially for microsystem applications in wireless sensor networks and on unmanned aerial vehicles (UAVs). To evaluate the rectenna designs, their rectifying efficiencies and compact sizes are two significant figures of merit. The antenna, which is typically bigger than the rectifying circuit, is one of the critical components of the rectenna system. On the one hand, the impedance matching between it and the rectifying circuit always affects the overall rectifying efficiency. Furthermore, its size typically dominates the overall size of the rectenna.

The basic structure of a rectenna is shown in Fig. 1(a). The antenna is the interface between the external electromagnetic (EM) environment and the rectifying circuit. It plays the significant role of receiving the EM signals and converting them into voltages and currents. Consequently, it also has important consequences in the requisite impedance matching to the rectifying circuit. The rectifying circuit consists of a band-pass filter, a Schottky diode, and a low pass filter. To increase the rectifying efficiency when the input power is low, a Schottky diode with a low built-in voltage and high breakdown voltage is always selected.[3] However, harmonic signals will be generated because the diode has nonlinear characteristics, and hence, could be radiated by the antenna back into the ambient space and absorbed by the board material. These harmonic generation and absorption processes can dramatically decrease the rectifying efficiency. Consequently, a band pass filter and a low pass filter are usually incorporated between the antenna and the diode, and between the diode and the load, respectively, to prevent any harmonics from flowing back into the antenna and forward into the load.

The emergence of metamaterials (MTMs) has provided a promising methodology to design electrically small antennas (ESAs).[4] The ESAs in Refs. 4 and 5 are constructed as a combination of electrically small driven and metamaterial-inspired near-field resonant parasitic (NFRP) elements. The NFRP elements are generally single epsilon-negative (ENG) or mu-negative (MNG) based unit cells of a metamaterial, not a complete bulk medium. In Refs. 6–8, an extended version of an S-shaped resonator has been found to yield a double negative (DNG) metamaterial (i.e., permittivity *and* permeability are negative). As a result, the S-shaped unit cell could be used as a NFRP element.

We combined such an S-shaped NFRP element and a driven printed monopole element to achieve an ESA that was matched to a 50 Ω and then directly to the input impedance of the rectifying circuit without any external matching network. Rather than a capricious choice for this proof-of-concept study, the GPS L1 frequency was selected because of past experiences with such narrow bandwidth systems[4,5] and the availability of related low and high power sources. Our rectenna design is based on 0.5-oz (0.017 mm thick copper), 31-mil (0.7874 mm), Rogers Duroid$^{\text{TM}}$ 5880 substrate ($\varepsilon_r = 2.2$, $\mu_r = 1.0$, and loss tangent = 0.0009) as the board material. The low input power, rectifying circuit design was based on the Skyworks SMS7630 Schottky diode. The agilent advanced design system (ADS) was exploited to design the rectifying circuit. Its harmonic balance (HB) simulator was selected to predict the rectifier performance, including the harmonics generation and the absorption process. To simplify the design of the low pass filter between the diode and the resistive load, an 82 nH series inductor was chosen to prevent the harmonics from reaching the load. From source pull and load pull simulation results in ADS, a 1540 Ω resistor was chosen as the resistive load to optimize the output power. The subsequent input impedance of the antenna was predicted to be $Z_{in} = (29.5 + j\ 171.55)\ \Omega$. Because this source impedance is an ideal value, it achieves the highest rectifying efficiency. This input impedance value was then used to design the ESA. The ADS circuit model of the optimized rectifying circuit is shown in Fig. 1(b).

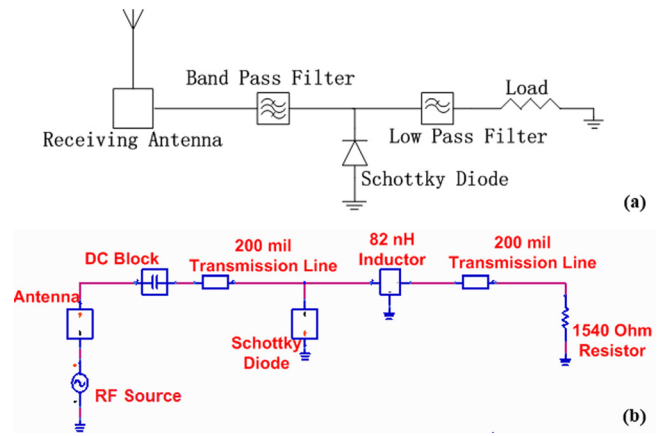a)Author to whom correspondence should be addressed. Electronic mail: ziolkowski@ece.arizona.edu.

FIG. 1. (Color online) Rectenna. (a) Basic structure and (b) ADS circuit model of its rectifying circuit.

TABLE I. Simulated performance characteristics of the rectenna.

Rectenna performance characteristics	Simulation results at 1.5754 GHz
Peak gain (dB)	1.063
Radiation efficiency (%)	66.5
1st Harmonic input impedance (Ω)	$44.9 + j\,167.0$
2nd Harmonic input impedance (Ω)	$322.0 + j\,183.0$
3rd Harmonic input impedance (Ω)	$76.0 - j\,24.0$
Rectifying efficiency at 0 dBm (%)	75.7

The electrically small, metamaterial-inspired S-shaped, NFRP antenna was designed using ANSYS/ANSOFT's high frequency structure simulator (HFSS). The design goals were an input impedance equal to $(29.5 + j\,171.55)\ \Omega$ while maintaining an electrically small size and high overall efficiency. The width and length of the S-shaped NFRP element provide the main contributions to the inductance of the antenna, while the distances between its vertical legs and the distances between its horizontal legs and the ground plane dominantly affect the capacitance of the antenna. Although there are several parameters available with the NFRP element to adjust the input impedance, it is nonetheless difficult to obtain the required high ratio of the reactance to the resistance, i.e., 5.8:1 (i.e., 171.55:29.5). We found that if the driven printed monopole was designed with a two-cane top-loading, this high impedance ratio could be obtained. Furthermore, we found that even though the antenna was physically separated from the circuit elements, the performance of the rectenna system was sensitive to the size of ground plane which is common to both the antenna and the rectifying circuit. The ground plane size itself is not negligible in comparison to the size of the S-shaped NFRP element. Consequently, to consider the ground plane effects on the antenna performance, we incorporated a same-sized ground plane without any of the circuit elements in the HFSS simulation model. Fig. 2(a) presents the antenna structure with the extended ground plane which was used to achieve its final design and whose one-port model was then used in the ADS simulations to optimize the rectifying circuit design. We note that the presence of the extended ground plane had to be de-embedded to the location of the input points of the actual rectifying circuit before creating the one-port model.

Fig. 2(b) shows the 3D radiation pattern of the S-shaped NFRP antenna predicted by HFSS. As one can see from Fig. 2(a), because the NFRP element is asymmetric with respect to the z-axis, the radiation pattern is tilted with respect to it and, hence, to the two-cane driven monopole. The simulated vector current distribution on the S-shaped NFRP element is presented in Fig. 2(c). One can see that the currents on the outside vertical legs of the S-shaped NFRP element flow in opposite directions to those on the middle vertical leg. Due to the resulting destructive interference of the fields generated by these opposite current flows, the radiation efficiency is only near 70%. Table I summarizes the HFSS predicted performance values, i.e., the simulated peak gain, the radiation efficiency, and the input impedance from fundamental through third harmonics, as well as the ADS predicted rectifying efficiency.

Combining and iterating between the rectifying circuit and antenna designs, we completed the rectenna design. The fabricated rectenna is shown in Fig. 3. The two-cane driven
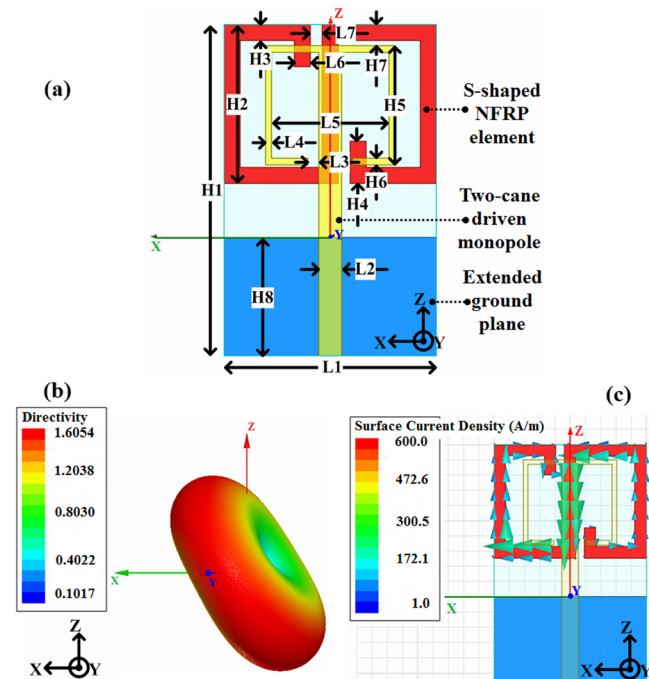

FIG. 2. (Color online) The GPS L1 antenna design, including the ground plane strip which has the same size as the rectifying circuit. (a) All dimensions are in millimeter: H1 = 31.176, H2 = 14.95, H3 = 1.5, H4 = 4, H5 = 11.2, H6 = 0.6, H7 = 3.9, H8 = 11.176, L1 = 20, L2 = 2.1336, L3 = 1.0732, L4 = 0.6, L5 = 11, L6 = 1.5, and L7 = 1.1; simulated (b) 3D radiation pattern and (c) vector current distribution on the S-shaped NFRP element at the GPS L1 frequency.

FIG. 3. (Color online) Front and back views of the fabricated GPS L1 rectenna. Left: two-cane driven monopole and rectifying circuit; right: S-shaped NFRP element and extended ground plane strip.
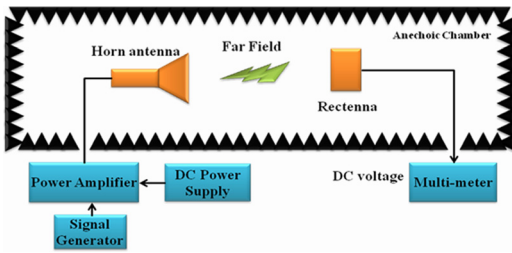
FIG. 4. (Color online) Rectenna measurement setup diagram.

monopole and rectifying circuit are on one side of the Duroid 5880 sheet, and the S-shaped NFRP element is on its other side.

The rectenna measurement setup is shown in Fig. 4. We physically fixed the tilt of the rectenna in the actual measurements to about 45°, corresponding to the maximum of the pattern shown in Fig. 2(c), to achieve the peak gain. The power delivered to the rectifying circuit (P_{input}) is calculated from the Friis transmission equation:[9]

$$P_{input} = \text{Effective Area} \times \text{Incident Power Density}$$
$$= G_r\left(\frac{\lambda^2}{4\pi}\right) \times \frac{G_t P_t}{4\pi R^2}, \tag{1}$$

where P_t is the power transmitted by the calibrated gain horn antenna, G_t is the gain of that horn antenna, G_r is the simulated gain of the S-shaped NFRP antenna, and R is the distance between the horn antenna and rectenna. After calculating the input power of the rectifying circuit, the final rectifying efficiency is determined as

$$\eta(\%) = \frac{V_L^2}{R_L} \times \frac{1}{P_{input}} \times 100, \tag{2}$$

where V_L is the DC voltage on the resistor and R_L is the resistor value.

The rectifying efficiencies were measured at various input powers when the frequency of the horn antenna was fixed at 1.5754 GHz and at a fixed input power: $P_{input} = 0.0$ dBm (1.0 mW), as the horn antenna frequency was scanned from 1.4 to 1.8 GHz. Comparisons of the measured and simulated power-dependent rectifying efficiencies are shown in Fig. 5(a). It indicates that the highest rectifying efficiency, 84.7%, was achieved at the GPS L1 frequency when P_{input} was 3.0 dBm, while the rectifying efficiency was 79.6% at GPS L1 frequency when P_{input} was 0.0 dBm. The measured efficiencies are slightly larger than their predicted values; simulations confirm that this difference falls within the tolerance values of the diode characteristics given by the manufacturer. Comparisons of the measured and simulated frequency-dependent rectifying efficiencies are shown in Fig. 5(b). It illustrates that the measured and simulated frequency-dependent results agree well with each other, especially at 1.5754 GHz. These measured results indicate that the metamaterial-inspired, S-shaped NFRP rectenna
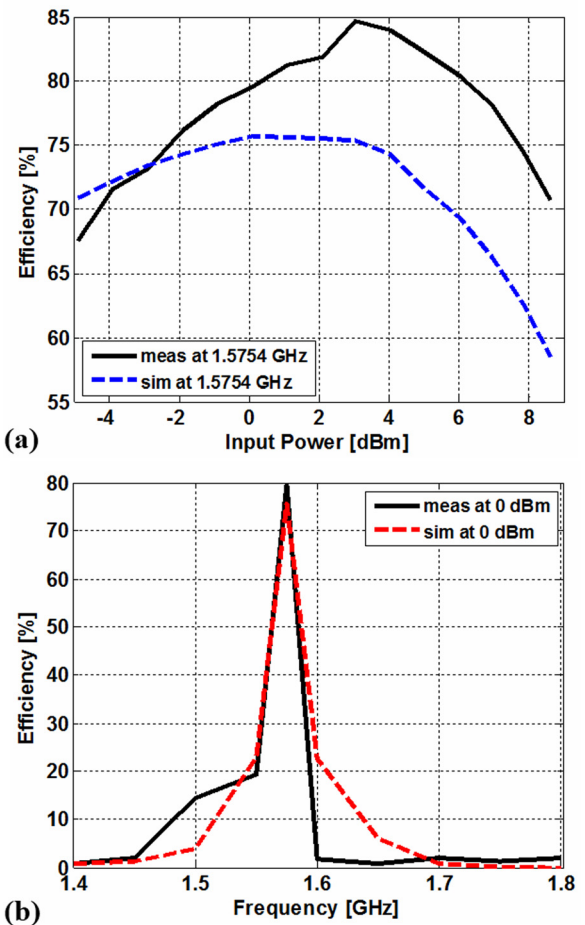

FIG. 5. (Color online) Measured and simulated results. (a) Rectifying efficiency at GPS L1 frequency versus input power at the rectifying circuit and (b) rectifying efficiency versus frequency when the input power of the rectifying circuit is 0.0 dBm.

achieves very high rectifying efficiency within an electrically small size. Electrically small rectennas analogous to this proto-typed example would be very good candidates for WPT applications such as power harvesting and scavenging systems.

[1]Y.-J. Ren and K. Chang, IEEE Trans. Microwave Theory Tech. **54**, 2970 (2006).
[2]J. O. McSpadden and J. C. Mankins, IEEE MICRO **3**, 46 (2002).
[3]N. Zhu, K. Chang, M. G. Tuo, P. Jin, H. Xin, and R. W. Ziolkowski, in *Proceedings of the IEEE Radio and Wireless Symposium* (IEEE, Piscatawy, NJ, 2011).
[4]R. W. Ziolkowski, P. Jin, and C.-C. Lin, "*Metamaterial-Inspired Engineering of Antennas*," Proc. IEEE (to be published).
[5]P. Jin and R. W. Ziolkowski, IEEE Trans. Antennas Propag. **59**, 1446 (2011).
[6]H. Chen, L. Ran, J. Huangfu, X. Zhang, K. Chen, T. M. Grzegorczyk, and J. A. Kong, J. Appl. Phys. **96**, 5338 (2004).
[7]H. Chen, L. Ran, J. Huangfu, X. Zhang, K. Chen, T. M. Grzegorczyk, and J. A. Kong, Phys. Rev. E **70**, 057605 (2004).
[8]L. Ran, J. Huangfu, H. Chen, X. Zhang, K. Cheng, T. M. Grzegorczyk, and J. A. Kong, Prog. Electromagn. Res. **51**, 249 (2005).
[9]C. A. Balanis, *Antenna Theory*, 3rd ed. (Wiley, New York, 2005).